ingegneria sismica
International Journal of Earthquake Engineering
Anno XLIII - Num. 3 - 2026

Seismic damage prediction of masonry structures: fusion of mathematical modeling and computer simulation

Yinghao Xu[1,*]

[1] College of Civil Engineering, Xi'an University of Architecture and Technology, Xi'an, Shaanxi, 710055, China

SUMMARY: *In response to the problem that traditional empirical statistical methods are difficult to accurately predict the degree of seismic damage to masonry structures and have a large deviation from actual seismic damage patterns, this paper takes a six story dormitory building with masonry on the bottom frame as the research object, and conducts seismic damage prediction and numerical simulation research. Firstly, a comprehensive modeling strategy is adopted to establish a finite element model of the masonry structure based on ABAQUS. The concrete damage plasticity (CDP) model is selected to describe the material constitutive behavior, and a three line hysteresis restoring force model considering stiffness degradation is introduced to characterize the interlayer mechanical properties; Secondly, the effectiveness of the model was verified through quasi-static experiments. Five amplitude modulated seismic waves were selected for dynamic elastoplastic time history analysis, and the seismic performance of the structure was evaluated based on plastic energy dissipation theory. The local deformation and energy dissipation laws of the wall under different construction measures were compared. Finally, experimental analysis shows that the fusion method of the established mathematical model and finite element simulation can accurately predict the evolution law of seismic damage in masonry structures. The construction of columns is a key measure to improve the seismic performance and collapse prevention ability of masonry structures. The research results can provide theoretical basis for seismic identification and reinforcement of masonry structures.*

KEYWORDS: *masonry structures; mathematical modeling; computer simulation; concrete damage plasticity (CDP); seismic damage prediction; quasi-static test; seismic performance*

1 Introduction

The prediction of building seismic damage is a fundamental prerequisite for urban earthquake prevention and disaster reduction work. The results of seismic damage prediction can be widely applied to the formulation of urban earthquake disaster prevention and reduction planning, the preparation of earthquake emergency response plans, and the implementation of existing building renovation and seismic reinforcement projects in cities [1-3]. Masonry structures are widely distributed in various parts of China and are widely used in the construction of densely populated building facilities such as residential buildings, schools, hospitals, and office buildings. The collapse and damage of brick masonry structures under earthquake action is the main cause of casualties in urban earthquake disasters [4-7]. Therefore, accurately predicting the severity of damage to masonry structures under different earthquake conditions, especially

*yinghaoxu0120@xauat.edu.cn
https://doi.org/10.65102/is20261205
Published: 10 June, 2026

clarifying their collapse risk to guide the scientific formulation of seismic reinforcement measures, has important theoretical and engineering practical significance for preventing and reducing casualties caused by earthquake disasters.

There are various methods for predicting seismic damage in masonry structures, such as statistical methods based on empirical damage, which are widely used due to their ease of operation [8-11]. The prediction results of earthquake damage are usually expressed in terms of damage levels, which are generally divided into five categories: intact, minor damage, moderate damage, severe damage, and destruction. The empirical damage prediction method calculates the damage index, compares it with actual damage data, and assigns specific damage levels to each index to determine the actual damage level of the structure [12-16]. When encountering a high-intensity earthquake, the prediction results of such methods show that there are almost no intact buildings in the masonry structure, and only a few slightly damaged buildings can withstand the action of a VII degree earthquake; Most masonry structures are expected to collapse or suffer severe damage, which deviates significantly from the actual seismic failure mode [17-20]. During a strong earthquake, some masonry structures with reasonable design and seismic resistance still exhibit good anti collapse performance in the area affected by an IX or X degree earthquake. However, the above empirical statistical methods clearly fail to fully capture this key feature [21, 22]. With the continuous development of artificial intelligence technology, the combination of mathematical modeling and computer simulation has gradually been applied in the field of earthquake damage prediction of building structures. Usually, only existing influencing factors related to structural damage need to be collected, and earthquake damage prediction results can be quickly generated through computer simulation [23-26].

Reference [27] focuses on analyzing the seismic vulnerability characteristics and failure laws of masonry structures under different earthquake magnitudes, and deeply analyzes their typical macroscopic damage characteristics and damage mechanisms. Reference [28] points out that masonry structures are the main carriers of significant damage during earthquakes, and clarifies the engineering value of accurately predicting seismic damage in masonry buildings. Reference [29] proposed a calculation model for quantifying the seismic performance enhancement effect of constrained components on restrained masonry structures, and validated it using on-site survey data from the Wenchuan earthquake. Reference [30] focuses on the damage characteristics of masonry structures in multi intensity zones, and through the analysis of the Wenchuan earthquake damage case, it is found that earthquake damage is mainly concentrated in the walls and building openings. Reference [31] studied the 2016 earthquake event in central Italy and proposed a damage prediction method for masonry structures based on peak ground acceleration. The feasibility and effectiveness of this method were verified. Reference [32] evaluated the post earthquake damage dataset of masonry buildings using machine learning models, which can effectively predict the seismic damage capacity of masonry structures. Reference [33] applied machine learning models to earthquake damage prediction and damage level classification of unreinforced masonry buildings, and found that Gaussian process regression models exhibited the best effectiveness in earthquake response prediction. Reference [34] evaluated the seismic damage of historical brick and stone buildings, and simulation research results confirmed that historical brick and stone buildings can fully withstand low-intensity seismic effects.

Reference [35] proposed a multi-level survey method that covers the investigation of masonry structure characteristics and the evaluation of building seismic performance. Reference [36] proposed a method for constructing a vulnerability matrix for masonry structures, providing reliable theoretical and methodological support for seismic damage

assessment and prediction of building groups. Reference [37] introduces a novel discrete modeling method suitable for seismic assessment of large structures, and verifies its effectiveness by applying it to seismic damage analysis of typical historical churches. Reference [38] studied the application of discrete element models and artificial neural networks (ANN) in seismic damage assessment of masonry reinforced concrete (RC) frames, which can effectively evaluate the seismic performance of filled masonry RC frames. Reference [39] explored the seismic response characteristics of severely damaged brick and stone school buildings during earthquakes, and provided the evolution laws and characteristics of building damage patterns after each main earthquake. Reference [40] introduced the construction of a prediction model for building damage intensity in mining environments, and verified the effectiveness of the proposed model in predicting the damage level of brick and stone residential buildings in mining areas. Reference [41] proposed a data-driven model for predicting the seismic vulnerability index of buildings based on standard design, which can assist decision-makers in allocating resources reasonably.

This study combines theoretical mathematical models with nonlinear finite element simulation techniques to conduct earthquake damage prediction analysis on actual masonry dormitory buildings. Selecting a dormitory building of a certain university as a typical case, this paper elaborates on its structural layout, material mechanics characteristics, and seismic design requirements in detail, clarifies the shortcomings of the measures in the construction process of the dormitory building, and deeply explores two finite element modeling methods. Combined with the core objective of macro level analysis in this study, a comprehensive modeling strategy that balances modeling efficiency and overall mechanical response capture ability is constructed. Then, the system elaborated on the damage mechanism, constitutive relationship, and determination method of key parameters of the concrete damage plasticity (CDP) model. Based on the structural layout characteristics and actual seismic damage characteristics of the "bottom frame upper masonry" of the dormitory building, a three tangent hysteresis restoring force model considering stiffness degradation is introduced to describe the hysteresis mechanical characteristics of the upper masonry layer. Specific calculation methods for stiffness, cracking load, yield load, and displacement at each stage are provided, and the material constitutive model and parameter value basis of the bottom frame concrete and steel reinforcement are clarified.

2 Finite Element Modeling and Material Constitutive Model Research

This study takes a certain university student dormitory building as the specific research object, systematically introduces the basic structural information and seismic design parameters of the dormitory building, clarifies its structural system characteristics and seismic design requirements, and constructs a finite element analysis model of the masonry structure. The core principles and parameter settings of the material constitutive model and restoring force model used in the model establishment process are elaborated in detail.

2.1 Case Structure Selection and Operating Condition Configuration

School buildings are highly densely populated areas, which are prone to causing mass casualties under earthquake action. This chapter selects a student dormitory building in a certain university as a typical research prototype for finite element simulation modeling. The specific information is as follows: The selected dormitory building is a six story masonry structure, built in 2012, with a single story height of 3.40 meters and a total construction area of 4132.93 square meters.

The engineering seismic fortification intensity is VII, the design basic seismic acceleration is 0.12g, the seismic design category is Class I, the seismic fortification category is Class C, the building site category is Class II, the structural safety level is Class II, the fire resistance level is Class II, and the foundation form adopts strip foundation. The wall is constructed using MU10 sintered ordinary bricks, with a strength grade of M10 cement mortar for the first and second layers, M7.5 cement mortar for the third and above layers, and a wall thickness of 250 mm. Ring beams with a cross-sectional size of 250 mm × 250 mm are installed on each floor, and HPB235 steel bars are used for reinforcement. The floor and roof slabs are both cast-in-place reinforced concrete slabs. The strip foundation is made of C15 rubble concrete, with a burial depth of 2.7 meters. Unless otherwise specified, the concrete strength grade of the main structure is C25. The structural load-bearing system is mainly supported by horizontal walls, and is jointly stressed by vertical and horizontal walls.

The architectural plan adopts the layout form of a central inner corridor and two side living rooms, with a living room opening of 4.2 meters and symmetrically arranged along the axis 16 as a whole. Structural columns are only installed at the four corners of the exterior wall, the entrance hall on the first floor, and the staircase. There are 24 structural columns on the first floor, and 18 structural columns on the second floor and above. In addition, the design drawings show that the structural columns at the inner corner of the staircase on axis 18 extend to the intersection of the inner longitudinal wall and axis 15. Multiple structural measures of the six story student dormitory do not meet the design requirements of the 8-degree seismic fortification zone in the 2003 version of the "Code for Seismic Design of Buildings", and some local components and structures cannot even meet the minimum specification requirements of the 7-degree seismic fortification zone.

2.2 Finite Element Model of Brick-Concrete Masonry Structures

This section focuses on the finite element modeling method for masonry structures, comparing the two modeling approaches of integrated modeling and decoupled modeling, and systematically explaining the theoretical basis, mechanical mechanism, and key parameter selection scheme for selecting the concrete damage plasticity (CDP) model in this paper.

2.2.1 Finite Element Modeling Method

Masonry structures are composed of composite materials of blocks and mortar, and their finite element modeling methods are mainly divided into two categories: (1) integrated models. Assuming that the wall is a continuous, uniform, and isotropic medium, the mortar is dispersed inside the wall, and the blocks and mortar are equivalent to a single homogeneous material, which has the characteristics of simplicity and efficiency and is suitable for dynamic response analysis of the overall wall and structural system level. (2) Separate model. The mortar layer is evenly distributed between adjacent blocks, and zero thickness interface elements are used to simulate the mechanical behavior of the mortar interface. The separated model can accurately simulate the cracking, debonding, and sliding failure behavior of the block mortar interface, and is widely used for material micromechanical performance analysis, including the study of tensile, compressive, and shear mechanical properties of masonry.

The core differences between the integrated model and the separated model are mainly reflected in three aspects: (1) The separated model is difficult to model, so independent units need to be established for the blocks and mortar, and the blocks need to be carefully arranged according to the actual masonry method of the wall; The integrated model homogenizes the blocks and mortar into an equivalent whole wall segment, making the modeling process simple and easy to operate. (2) The integrated model unit has fewer contact interfaces, resulting in higher computational efficiency under reasonable grid partitioning conditions; There are a large

number of contact interfaces between the separated model blocks, which significantly increases the calculation time. (3) The integrated model can identify the location of wall cracking and the development of damage through equivalent plastic strain cloud maps; The separated model can intuitively reflect the sliding and cracking characteristics between blocks in the deformation results, and can finely simulate the entire process of crack initiation and propagation. Based on the positioning of this research, this article ultimately chooses the integrated modeling method to carry out finite element modeling analysis.

2.2.2 Plastic Damage Model for Concrete

When conducting finite element numerical analysis of masonry structures, the reasonable selection of material parameters and constitutive relationships has a decisive impact on the accuracy of simulation results. The analysis parameters and material constitutive relationships used in this study are comprehensively determined based on current standards and mature research results.

ABAQUS does not provide a dedicated mechanical model for masonry materials. However, it offers three mechanical models for concrete under low confining pressure: the Concrete Damage Plasticity (CDP) model, the Brittle Cracking (BC) model, and the Concrete Scattered Cracking (CSC) model. Among these, the Concrete Scattered Cracking (CSC) model is suitable for simulating members subjected to low confining pressure under monotonic loading; the Brittle Cracking (BC) model is exclusively used in display analyses to simulate materials primarily prone to tensile failure; The Concrete Damage Plasticity (CDP) model incorporates damage effects and is suitable for simulating various mechanical behaviors under monotonic, cyclic, and seismic loading. The CDP model, which accounts for the difference in tensile and compressive properties of materials, is used to simulate irreversible degradation caused by material damage. This degradation manifests primarily in: differing tensile and compressive yield strengths for macroscopic properties; distinct damage factors for tensile and compressive loading; material softening after tensile yielding; material strengthening followed by softening after compressive yielding; and partial stiffness recovery under cyclic loading. The broad applicability of the CDP model extends beyond simulating concrete mechanics to include numerical analysis of masonry. Therefore, this paper employs the CDP model to establish the constitutive relationship for brick masonry.

The CDP model employs a two-parameter DP failure criterion, assuming tensile cracking and compressive crushing as the primary causes of damage in concrete materials. By introducing tensile damage factor d_t and compressive damage factor d_c into the tensile and compressive constitutive relationships of the material, research indicates that the concrete damage plasticity model effectively simulates tensile fracture and compressive failure processes in brittle materials such as concrete and masonry. Under uniaxial tension, the damage-free linear elastic stage persists until the peak tensile stress σ_{t0} is reached, after which the damage-induced softening stage commences. Under uniaxial compression, the undamaged linear elastic stage persists until the peak compressive stress σ_{c0} is reached, followed by a damage-induced strengthening phase. Upon reaching the peak compressive stress σ_{cu}, the material enters the softening stage. The elastic modulus of a material after damage degradation during the softening phase under tension or compression can be described by the initial elastic modulus E_0 and the damage factor:

$$E' = (1-d)E_0 \tag{1}$$

The plastic strain at any point on the tensile softening segment after unloading at the initial stiffness is referred to as the cracking strain:

$$\varepsilon_t^{ck} = \varepsilon_t - \frac{\sigma_t}{E_0} \tag{2}$$

If unloading is performed based on the reduced stiffness, the plastic strain after unloading is referred to as the tensile equivalent plastic strain:

$$\varepsilon_t^{pl} = \varepsilon_t^{ck} - \frac{d_t}{1-d_t}\frac{\sigma_t}{E_0} \tag{3}$$

At the same time, the plastic strain at any point on the compressed softening section after unloading at the initial stiffness is referred to as inelastic strain:

$$\varepsilon_c^{in} = \varepsilon_c - \frac{\sigma_c}{E_0} \tag{4}$$

If unloading is performed based on the reduced stiffness, the plastic strain after unloading is referred to as the compression-equivalent plastic strain:

$$\varepsilon_c^{pl} = \varepsilon_c^{in} - \frac{d_c}{1-d_c}\frac{\sigma_c}{E_0} \tag{5}$$

The ε_t^{pl} and ε_c^{pl} control the evolution of the damage surfaces of the material, and only the "tensile stress σ_t, cracking strain ε_t^{ck}, tensile damage factor d_t" and "compressive stress σ_c, cracking strain ε_c^{in}, tensile damage factor d_c", which can be transformed into real stress-strain into real stress-strain relationship.

In this paper, the energy method is used to derive the damage factor, based on the principle of energy equivalence, the elastic residual energy produced by stress acting on damaged materials has the same form as the elastic residual energy produced by acting on uninjured materials, as long as the simple replacement of the stress for the effective stress or replacement of elastic modulus for the equivalent elastic modulus after damage, the damage factor calculated by this method is:

$$d = 1 - \sqrt{\frac{\sigma}{E_0 \varepsilon}} \tag{6}$$

2.3 Modeling of interlayer restoring forces and material principal relationships

Based on the aforementioned finite element modeling method, this section further addresses the seismic damage characteristics of the bottom frame and the upper masonry in the case structure, and proposes the interstory restoring force model and material constitutive relationship applicable to the structure, which provides a mechanical basis for the subsequent seismic response simulation.

The actual damage of the case structure is mainly located in the bottom G-axis frame columns and the infill wall, and the damage in other locations is slight. In this paper, the G-axis bottom frame and the upper masonry are selected as the research objects, and the upper masonry structure is simplified into a multi-degree-of-freedom system, while the frame structure of the lower infill wall is modeled in a refined way to focus on the damage process of the bottom frame under seismic action.

2.3.1 Masonry interlayer restoring force modeling

The upper part of the base frame masonry structure is load-bearing by brick masonry, and the selection of an appropriate restoring force model for brick masonry is the basis for nonlinear seismic response analysis. Horizontal low-period reciprocation tests of the masonry wall fragments showed that the hysteresis curve of the brick wall showed a “shuttle” shape, which was characterized by a shear damage mode. The wall undergoes four stages from stress to complete damage: elastic stage, elasto-plastic cracking stage, load drop damage section and friction slip section. In this paper, the triple-fold restoring force model considering stiffness degradation is chosen to simulate the dynamic response of the upper masonry under earthquake, and its skeleton curve is shown in Fig. 1.

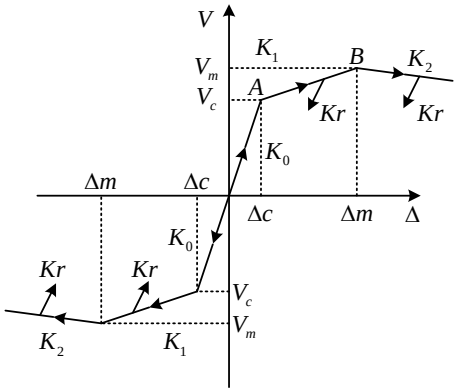

Figure 1: Skeleton curve

In the figure, K_0 represents the initial lateral stiffness before cracking; point A denotes the cracking point, Δ_c indicates the cracking lateral displacement, and V_c signifies the cracking load; K_1 denotes the lateral stiffness after cracking but before yielding; Point B is the yield point, Δ_m is the yield lateral displacement, V_m is the yield load; K_2 is the degradation stiffness after yielding; Kr is the unloading stiffness.

Initial elastic lateral stiffness of masonry walls with structural columns

$$K_0 = \lambda_m \frac{GA_m}{\mu h} \tag{7}$$

In the formula: G is the shear modulus of masonry, taken as $0.4E$; A_m is the horizontal gross cross-sectional area of the masonry wall; μ is the coefficient of shear stress distribution unevenness, taken as 1-2 for rectangular cross-sections; h is the masonry course height; λ_m is the stiffness correction factor for walls with structural columns, accounting for openings.

Lateral stiffness from cracking to yielding

$$K_1 = (0.188 - 0.031\sigma_0)K_0 \tag{8}$$

Lateral stiffness after yielding

$$K_2 = -(0.188 - 0.031\sigma_0)K_0 \tag{9}$$

Unloading stiffness after interlayer displacement exceeds cracking displacement and enters the yield segment

$$K_r = \left(\frac{\Delta_r}{\Delta_c}\right)^{-0.85} K_0 \tag{10}$$

The cracking load of masonry is

$$V_c = \zeta f_v (1 + \frac{\sigma_0}{f_v})^{0.5} A_m \tag{11}$$

In the formula: σ_0 represents the average compressive stress generated by self-weight at half the floor height; ζ is the adjustment coefficient accounting for structural columns and non-uniform shear stress distribution, taken as 1.07; f_v denotes the shear strength of brick masonry; A_m indicates the horizontal gross cross-sectional area of the wall.

Corresponding cracking lateral displacement

$$\Delta_c = V_c / K_0 \tag{12}$$

The shear bearing capacity and yield displacement at yield are respectively

$$V_m = 1 - 125V_c, \Delta_m = \Delta_c + (V_m - V_c)/K_1 \tag{13}$$

Maximum displacement is

$$\Delta_u = 5\Delta_c \tag{14}$$

2.3.2 Material Constitutive Relations

Actual seismic damage revealed cracking and fragmentation of concrete in frame columns, indicating significant damage. This article uses the concrete damage plasticity (CDP) model to characterize the mechanical properties of concrete.

The CDP model integrates the fracture damage and stiffness degradation mechanisms in continuous damage mechanics theory to construct a continuous isotropic damage constitutive model. By using two independent damage variables, compressive damage and tensile damage, combined with a yield criterion controlled by multiple hardening variables, the damage evolution state of materials at different stress stages is accurately characterized. This model describes the degradation process of initial elastic stiffness caused by plastic strain, making it suitable for simulating the highly nonlinear behavior of concrete under tensile cracking and compressive crushing during cyclic loading.

The specific parameter settings for the model are as follows: the shear dilation angle ψ on the plane of shear is set to 30°; the eccentricity e of the plastic flow potential is 0.12; the ratio of biaxial compressive strength to uniaxial compressive strength f_{10} / f_0 is set to 1.14; and the viscosity coefficient μ is 0.0001.

The uniaxial tensile-compressive constitutive model for concrete is selected from the segmented concrete constitutive model recommended in the "Code for Design of Concrete Structures." Its compression segment expression is:

$$\begin{cases} y = \alpha_a x + (3 - 2\alpha_a)x^2 + (\alpha_a - 2)x^3 & x \le 1 \\ y = \dfrac{x}{\alpha_d (x-1)^2 + x} & x > 1 \end{cases} \tag{15}$$

In the equation: $x = \varepsilon / \varepsilon_c, y = \sigma / f_c^*$; f_c^* denotes the uniaxial compressive strength of concrete, taken as the average compressive strength f_{cm} in this paper; ε_c represents the peak compressive strain corresponding to $f_c^{'}$; α_{a} and α_d are the parameter values for the ascending and descending segments of the uniaxial compression stress-strain curve, respectively, selected according to the code.

The tensile segment expression is

$$\begin{cases} y = 1 - 2x - 0.2x^6 & x \le 1 \\ y = \dfrac{x}{\alpha_d (x-1)^{1-7} + x} & x > 1 \end{cases} \tag{16}$$

where: $x = \varepsilon / \varepsilon_1, y = \sigma / f_1^e$; f_1^e is the uniaxial tensile strength of concrete, and in this paper we take the average value of tensile strength f_m; ε_1 is the peak tensile strain of concrete corresponding to $f_1^{'}$; and α_i is the parameter value of the descending section of the uniaxial tensile stress-strain curve, which is selected according to the code.

The concrete damage factor is a function of the stress state and plastic strain, and its expression is given by

$$d_k = 1 - \frac{\sigma_k E_0^{-1}}{\varepsilon_k^{pl}(1/b_k - 1) + \sigma_k E_0^{-1}}, k \text{ is } c \text{ or } t \tag{17}$$

$$\varepsilon_k^{pl} = b_k \varepsilon_k^{in} \tag{18}$$

$$\varepsilon_k^{in} = \varepsilon_k - \sigma_k E_0^{-1} \tag{19}$$

In the equation: c denotes compression, t denotes tension; E_0 denotes the initial elastic modulus of concrete, taken as the tangent modulus at tensile cracking; ε_t^{μ} denotes plastic strain; ε_k^{im} denotes inelastic strain; b_k represents the ratio of plastic strain to inelastic strain, taken as 0.7 for compression and 0.1 for tension.

The uniaxial stress-strain relationship of reinforcement adopts a multi-polyline constitutive model under cyclic loading. This model reflects the degradation process of bending member

capacity caused by cumulative damage. The constitutive model for reinforcement is shown in Figure 2.

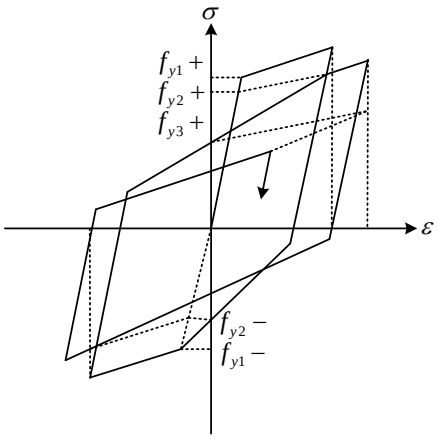

Figure 2: Constitutive model for reinforcement

Masonry is a two-phase anisotropic material constructed by arranging blocks in a specific pattern. The determination of masonry constitutive relationships is primarily based on results from planar uniaxial loading tests, focusing on its compression failure criteria and stress-strain relationship. In ABAQUS finite element software, the mechanical properties of masonry are still simulated using concrete damage-plasticity models. For the compressed section of masonry, the uniaxial compression constitutive model proposed by Yang Weizhong based on the damage characteristics of masonry under compression is employed. Its expression is:

$$\frac{\sigma}{f_m}=\frac{\eta}{1+(\eta-1)(\varepsilon/\varepsilon_m)^{\eta/(\eta-1)}}\frac{\varepsilon}{\varepsilon_m} \tag{20}$$

In the equation: η is taken as 1.629, f_m is the average uniaxial compressive strength of masonry, and ε_m is the strain corresponding to f_m.

The axial tensile strength of masonry is very low, and tensile failure manifests as mortar joint cracking, exhibiting brittle failure. The uniaxial tensile stress-strain curve for masonry is difficult to obtain experimentally. However, since the tensile failure characteristics of masonry are similar to those of concrete, the tensile constitutive relationship of concrete can be used to approximate the uniaxial tensile stress-strain relationship of masonry.

3 Finite Element Simulation Verification of Seismic Performance and Earthquake Damage Prediction Analysis for Masonry Structures

The integrated modeling method, CDP material constitutive model, and trilinear hysteresis restoring force model have been constructed in the previous section. This chapter further carries out numerical simulation and result analysis work: (1) By comparing with quasi-static test results, the effectiveness and accuracy of the model are verified; (2) Apply the validated model to systematically analyze the impact of various structural measures on the seismic performance of the structure; (3) Conduct a comprehensive evaluation of the plastic energy dissipation characteristics and seismic damage of masonry structures under seismic loads.

3.1 Numerical Simulation of Seismic Damage in Masonry Structures

Based on the principles and settings of parameters required for finite element modeling of masonry structures, as well as the constitutive relationships of various materials introduced in the preceding sections, this chapter employs ABAQUS finite element software to conduct numerical simulations of brick masonry walls. The computational results are compared with those from quasi-static tests, with experimental data used to refine relevant modeling parameters. Ultimately, this approach validates the rationality and accuracy of modeling brick masonry walls using ABAQUS finite element software.

3.1.1 Model Primary Material Parameter Settings

A brick masonry wall model was established based on the article. The concrete material strength grade is C25, with an elastic modulus of 2.63×10^4 N/mm² and a Poisson's ratio of 0.25. Substituting these values into the relevant formula, and considering that this paper approximates the uniaxial tensile stress-strain relationship of masonry using the tensile constitutive relationship of concrete, the calculated plastic damage parameters for the masonry structural material under compression and tension are shown in Table 1 below.

Table 1: Tensile parameters of plastic damage model for masonry structure materials

Stress	Cracking strain	Tensile equivalent plastic strain	Non-elastic strain	Compressive equivalent plastic strain	Loss factor
3.50E+01	0.00E+00	0.00E+00	0.00E+00	0.00E+00	0.00E+00
3.72E+01	1.23E-03	1.00E-03	1.34E-03	1.17E-03	3.45E-01
3.82E+01	1.65E-03	1.35E-03	1.64E-03	1.46E-03	3.78E-01
3.86E+01	1.82E-03	1.83E-03	1.90E-03	1.77E-03	4.12E-01
3.81E+01	2.17E-03	2.12E-03	2.23E-03	2.32E-03	4.45E-01
3.73E+01	2.41E-03	2.40E-03	2.55E-03	2.35E-03	4.78E-01
3.62E+01	2.04E-03	2.74E-03	2.85E-03	2.64E-03	5.10E-01
3.48E+01	3.13E-03	3.03E-03	3.13E-03	2.99E-03	5.42E-01
3.34E+01	3.43E-03	3.34E-03	3.43E-03	3.21E-03	5.73E-01
3.19E+01	3.62E-03	3.63E-03	3.71E-03	3.56E-03	6.02E-01
3.04E+01	3.94E-03	3.93E-03	4.08E-03	3.87E-03	6.34E-01
2.90E+01	4.28E-03	4.22E-03	4.33E-03	4.19E-03	6.56E-01
2.76E+01	4.59E-03	4.51E-03	4.65E-03	4.44E-03	6.85E-01
2.63E+01	4.84E-03	4.83E-03	4.92E-03	4.77E-03	7.02E-01
2.20E+01	6.01E-03	6.56E-03	6.17E-03	5.93E-03	7.45E-01
1.87E+01	7.26E-03	7.29E-03	7.31E-03	7.10E-03	7.82E-01
1.73E+01	7.85E-03	7.86E-03	7.98E-03	7.75E-03	8.54E-01
1.41E+01	9.65E-03	9.06E-03	9.75E-03	9.50E-03	8.35E-01
1.26E+01	1.09E-02	1.08E-02	1.07E-02	1.07E-02	8.62E-01
1.13E+01	1.21E-02	1.20E-02	1.22E-02	1.19E-02	8.82E-01
1.02E+01	1.33E-02	1.32E-02	1.34E-02	1.31E-02	8.95E-01
9.35E+00	1.45E-02	1.44E-02	1.46E-02	1.43E-02	9.08E-01
8.61E+00	1.57E-02	1.56E-02	1.58E-02	1.55E-02	9.22E-01
7.98E+00	1.69E-02	1.68E-02	1.76E-02	1.67E-02	9.38E-01
7.42E+00	1.81E-02	1.83E-02	1.82E-02	1.79E-02	9.46E-01
6.94E+00	1.93E-02	1.92E-02	1.94E-02	1.91E-02	9.48E-01
6.52E+00	2.05E-02	2.04E-02	2.06E-02	2.03E-02	9.56E-01
6.14E+00	2.17E-02	2.16E-02	2.18E-02	2.15E-02	9.63E-01
5.81E+00	2.29E-02	2.28E-02	2.30E-02	2.27E-02	9.71E-01
5.51E+00	2.41E-02	2.42E-02	2.42E-02	2.39E-02	9.76E-01

Table 1 presents the core parameters of the concrete damage plasticity (CDP) model for masonry materials under uniaxial tension and compression. According to the experimental data in Table 1, the proposed model can fully describe the mechanical behavior of the material throughout the entire process: (1) under tensile conditions, the initial stress is 35.00 MPa, and the material is in the non-destructive linear elastic stage; (2) The cracking strain and inelastic strain continue to develop, and the tensile stress rises to a peak of 38.60 MPa before entering the softening stage, gradually decreasing to 5.51 MPa. The corresponding tensile damage factor increases monotonically from 0 to 0.976, clearly reflecting the typical brittle characteristics of masonry materials. Under compressive conditions, the stress-strain curve also exhibits a linear increase and gradual softening after reaching its peak; The compressive damage factor continues to increase with the accumulation of equivalent plastic strain, reflecting the evolution process of compressive damage characterized by the continuous expansion of microcracks inside the material and the continuous deterioration of macroscopic mechanical properties.

3.1.2 Analysis of Retention Characteristics Results

After completing the modeling of the brick masonry wall, select the center loading point on the left side of the ring beam, couple the horizontal load and horizontal displacement, and extract response data to analyze the cumulative law of plastic strain of the wall and the evolution characteristics of surface crack propagation of the component during the gradual increase of horizontal load. By comparing the numerical simulation results with the indoor quasi-static test results, the rationality and accuracy of the constitutive parameters, interface bonding, and contact behavior settings of masonry, steel bars, and concrete materials in the finite element model are verified. Figure 3 shows the comparison curve between the quasi-static test results and the finite element numerical simulation results of the QG wall component with ring beams and structural columns as the research object.

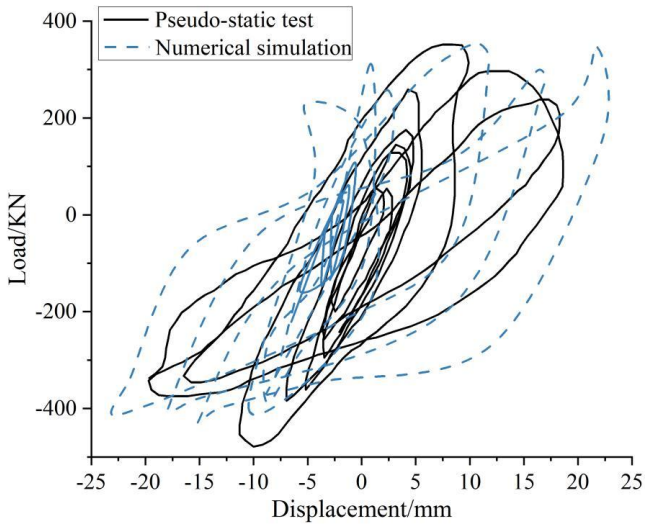

Figure 3: Comparison of the pseudo-static and numerical simulation test results

From the comparison results shown in Figure 3, it can be seen that both the experimental measurement and numerical simulation show a spindle shaped hysteresis loop, indicating that the QG component has good energy dissipation and shock absorption performance. The numerical simulation results are highly consistent with the experimental results, verifying the accuracy and reliability of using this finite element modeling method to analyze the stress response of masonry components.

Figures 4 and 5 respectively show the comparison results of the skeleton curve and stiffness

degradation curve obtained from numerical simulation and experimental measurement of QG components. From the experimental results in Figures 4 and 5, it can be seen that during the initial loading stage and yielding stage of the component, the simulated curve basically overlaps with the experimental curve. After entering the failure stage, the numerical simulation skeleton curve is slightly lower than the experimental skeleton curve, and the relative error between the two is less than 3%. Ultimately, failure occurs when the load reaches approximately 90% of the peak load. Overall, the finite element simulation results are in good agreement with the experimental data. The simulated values indicate that the stiffness degrades to 85 kN/mm after 8 hysteresis cycles, consistent with the final stiffness degradation observed in the actual experiments.

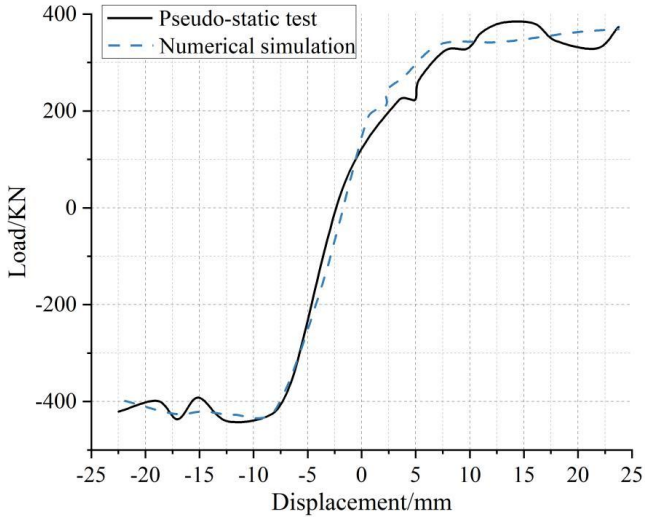

Figure 4: Component QG skeleton curve

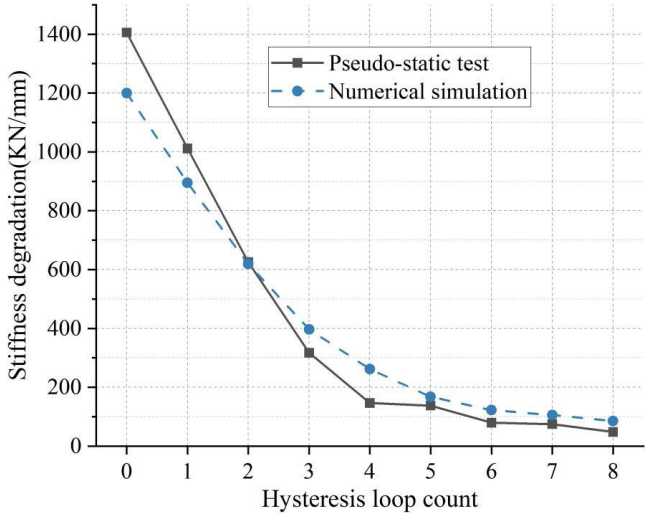

Figure 5: The stiffness degradation curve of component QG

3.1.3 Comparison of Masonry Wall Performance Under Different Construction Measures

Through analyzing the retention characteristics of wall component QG, which incorporates a ring beam and structural columns, to further examine the impact of reinforcement configurations in structural columns and ring beams on the wall, we now continue using the aforementioned finite element modeling method to simulate four brick masonry wall specimens

with identical material properties but differing structural measures, all containing only ring beams. The specific designs are as follows.

Specimen 1: Component QG-1 studied above, containing a ring beam and structural columns, with ring beam longitudinal reinforcement of 2Φ12 and stirrups of Φ6@200; structural column longitudinal reinforcement of 2Φ12 and stirrups of Φ6@250;

Specimen 2: Component QG-2 with ring beam and structural column. The ring beam configuration is identical to Specimen 1. The structural column has longitudinal reinforcement of 2Φ14 and stirrups of Φ6@200.

Specimen 3: Component Q-1 containing only a ring beam. The ring beam has longitudinal reinforcement of 2Φ12 and stirrups of Φ6@200.

Sample 4: Component Q-2 contains only one ring beam, with longitudinal reinforcement of 2 Φ 14 and hoop reinforcement of Φ 6 @ 150.

Figure 6 shows a comparison of hysteresis curves for four cases with the same material properties but different structural measures under horizontal cyclic loading.

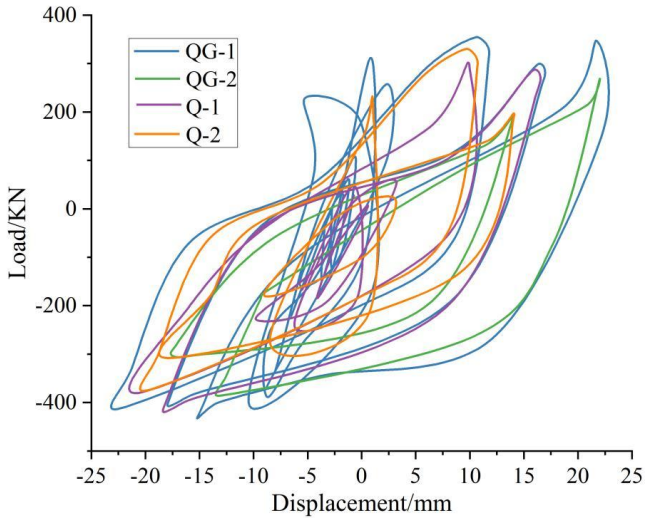

Figure 6: Hysteresis curves of masonry walls under different constructions

From the comparison results shown in Figure 6, it can be seen that the slopes of each curve are basically the same in the initial elastic stage. After entering the plastic stress stage, the hysteresis loop of the specimen with the structural column is more full, and the peak load is significantly increased. The QG-2 specimen has a significant increase in peak bearing capacity due to the strengthening of the longitudinal steel reinforcement of the structural column. However, only optimizing the ring beam steel reinforcement has a very weak effect on the hysteresis loop shape.

Comparative analysis of four models with different structural measures shows that compared to specimens without structural columns, the energy dissipation capacity of brick masonry walls with structural columns is significantly improved; The influence of horizontal reinforcement of ring beams on hysteresis performance can be basically ignored. Improving the longitudinal reinforcement ratio of structural columns and reducing the spacing between stirrups can effectively enhance the peak load and initial stiffness of hysteresis curves. The above pattern indicates that the improvement effect of reinforcing steel bars in structural columns on the seismic performance of walls is far superior to simply strengthening steel bars in ring beams, verifying the dominant role of structural columns in enhancing the energy dissipation capacity of walls.

3.2 Seismic Performance Analysis of Masonry Structures Based on Plastic Energy Dissipation

By systematically analyzing the hysteresis performance, skeleton curve, and stiffness degradation law of single masonry wall components, the effectiveness and accuracy of the finite element numerical method based on ABAQUS and CDP models in simulating the nonlinear mechanical behavior of masonry structures were successfully verified, and the comprehensive seismic performance of the dormitory building under actual seismic input was evaluated. This section selects multiple natural seismic waves to conduct dynamic elastic-plastic time history analysis on the dormitory building, and finally conducts in-depth quantitative evaluation of the overall seismic performance of the structure based on plastic energy dissipation theory.

3.2.1 Selection of Seismic Motion Records

This study selected a total of 5 natural earthquake motion records and adjusted the amplitude of the earthquake motion to the seismic fortification intensity level of 7 degrees, corresponding to magnitudes of 7.10, 7.15, 7.20, 7.25, and 7.30, respectively. The duration of earthquake motion has a significant impact on the seismic response of structures, and the conventional values include the peak ground acceleration period, which is 5-10 times the basic natural period of the structure. This article uses seismic waves with a duration of 5 seconds for analysis. The comparison results between the seismic response spectrum and the standard design response spectrum are shown in Figure 7.

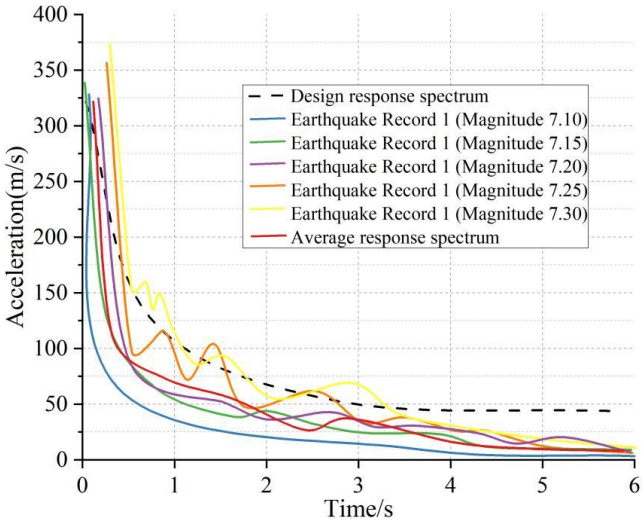

Figure 7: Comparison curve between the measured seismic response spectrum and the design response spectrum specified in the specifications

Figure 7 clearly presents the seismic response spectra corresponding to seismic records in various regions. The experimental results in Figure 7 indicate that the selected seismic waves can effectively reflect the design seismic action under a seismic fortification intensity of 7 degrees. This verification result ensures that the seismic parameters input for subsequent dynamic time history analysis meet the requirements of the specifications.

3.2.2 Plastic Energy Dissipation Analysis of Structures Under Seismic Loading

Based on the seismic response characteristics of structures with different levels of damage, the weaker the nonlinear hysteresis energy dissipation capacity of the structure, the more severe the damage will be under the same seismic action. Figures 8, 9, and 10 show the plastic energy

dissipation time history curves of the structure under the action of five seismic waves, corresponding to three levels of slight damage, moderate damage, and severe damage.

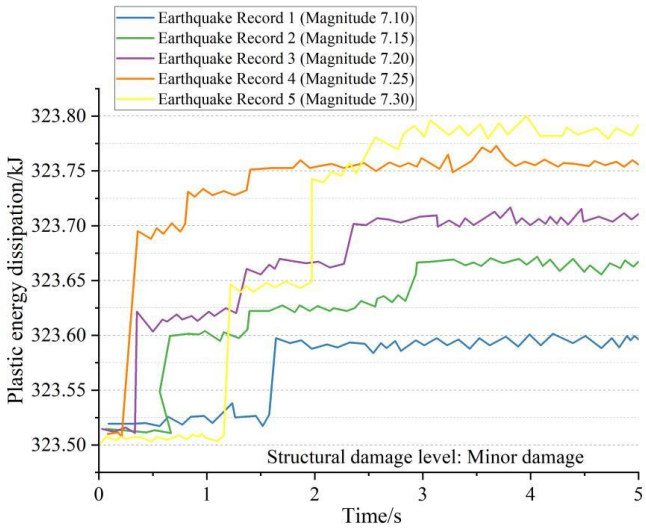

Figure 8: Plastic energy dissipation time-history curve under minor damage

At the level of minor damage, a small amount of plastic energy dissipation is generated during the initial loading stage due to the influence of initial structural defects. The overall curve trend is gentle and shows a stepped growth, and the structure mainly responds elastically, with only local microcrack propagation occurring. The level of plastic energy dissipation is below the critical threshold for damage, which is consistent with the characteristics of slight damage stress. Seismic energy is mainly dissipated by damping rather than plastic deformation dissipation.

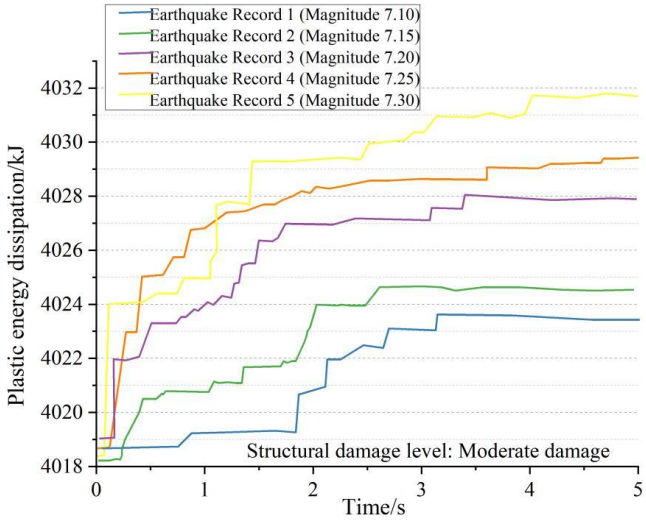

Figure 9: Plastic energy dissipation time-history curve under moderate damage

At moderate damage levels, the plastic energy dissipation of the structure significantly increases, with a noticeable increase in the initial segment of the curve and a brief plateau characteristic, reflecting the coexistence of the elastic recovery effect and plastic energy dissipation of the structure. The peak plastic energy dissipation can reach more than three times that of the mild damage condition, indicating that some components have entered the yield stress stage, and the damage continues to accumulate and cause structural stiffness degradation,

but the main structure still retains a certain vertical and horizontal bearing capacity.

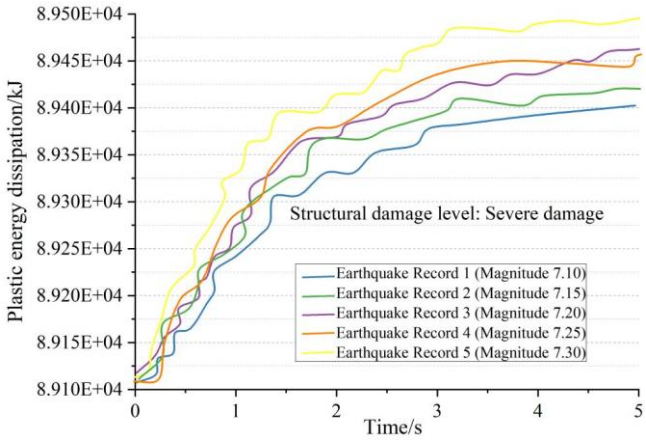

Figure 10: Plastic energy dissipation time-history curve under severe damage

Under severe damage levels, the plastic energy dissipation process shows an exponential growth with no obvious linear elastic stage, indicating that the structure has completely entered a plastic stress state, causing damage phenomena such as concrete crushing and steel buckling of the bottom floor frame columns. Seismic energy is mainly dissipated through plastic energy dissipation.

Figures 8, 9, and 10 clearly reflect the significant differences in plastic energy dissipation of structures under different levels of damage. The structure gradually enters the stage of plastic development under earthquake action, and when it loses its elastic recovery ability and relies solely on plastic deformation for energy dissipation, it already has the risk of collapse.

3.3 Study on Local Deformation Patterns of Test Specimens

This section focuses on the analysis of local deformation patterns and relative displacement changes of measuring points of walls under different structural measures from the perspective of overall structure regression. The macroscopic energy dissipation characteristics are combined with microscopic deformation and failure mechanisms to fully explain the entire process of structural seismic failure evolution from multiple dimensions. The research object is symmetrically arranged reinforced masonry walls. Subsequently, comparative analysis will be conducted on four groups of specimens, QG-1, QG-2, Q-1, and Q-2.

3.3.1 Characteristics of Variations in Wall Height Spacing

Wall component QG-1 is equipped with 2 Φ 12 longitudinal steel bars, with a displacement loading amplitude increment of 5.0 mm; wall component QG-2 is equipped with 2 Φ 14 longitudinal steel bars, with a displacement loading amplitude increment of 2.0 mm. Displacement conditions Δ=+2.0 mm and Δ=+25.0 mm are selected for research. Tables 2 and 3 show the displacement responses of each specimen at different heights of measurement points under two working conditions: considering prestress and not considering prestress; Figures 11 and 12 correspond to the deformation distribution curves of the wall along the height under two different working conditions.

Table 2: Displacements of each specimen at different heights under prestress

	H/mm	QG-1-A	QG-1-B	QG-2-A	QG-2-B
△=+2.0 mm	800	1.25	-1.18	3.32	-3.29
	1000	2.67	-2.54	6.81	-6.73
	1200	3.89	-3.75	8.12	-8.05
	1400	4.93	-4.82	11.23	-11.11
△=+25.0 mm	800	12.36	-11.89	13.45	-13.22
	1000	18.74	-18.25	19.83	-19.41
	1200	22.56	-21.98	23.67	-23.12
	1400	26.33	-25.81	27.45	-26.94

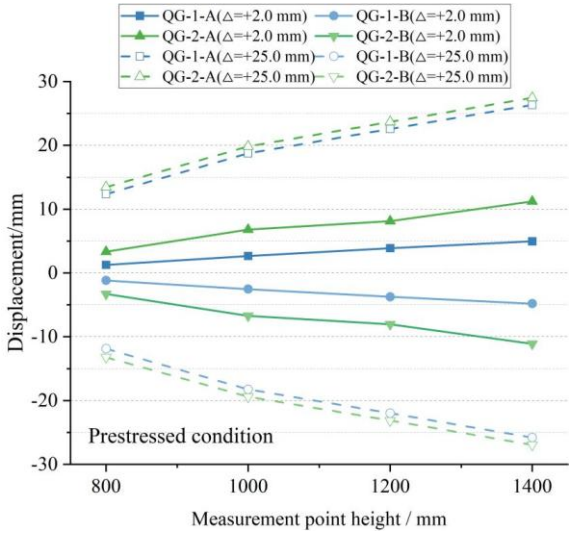

Figure 11: Deformation diagram of wall height under prestressed condition

Under prestressing conditions, QG-2 exhibits higher displacement values at the same height and loading conditions. At 1400mm, when △=+25.0mm, QG-2 shows 27.45mm displacement versus QG-1's 26.33mm. The overall deformation curve in Figure 11 is relatively smooth and flat, indicating that prestressing can suppress the initiation and propagation of initial cracks in the wall, making the deformation distribution of the wall more uniform. However, the overall deformation amplitude of the structure is still relatively large, indicating that prestressing has not completely eliminated the plastic response of the structure. The deformation capacity of the QG-2 specimen has significantly improved due to the reinforcement of its structural columns, effectively improving the energy dissipation performance and overall seismic performance of the wall.

Table 3: Displacements of each specimen at different heights without prestress

	H/mm	QG-1-A	QG-1-B	QG-2-A	QG-2-B
△=+2.0 mm	800	1.87	-1.79	2.95	-2.88
	1000	3.45	-3.32	4.62	-4.51
	1200	5.12	-4.98	6.34	-6.21
	1400	6.78	-6.64	8.03	-8.89
△=+25.0 mm	800	14.21	-13.85	15.12	-14.87
	1000	21.45	-20.89	22.67	-22.13
	1200	23.78	-25.12	24.94	-26.35
	1400	26.63	-28.94	27.82	-29.11

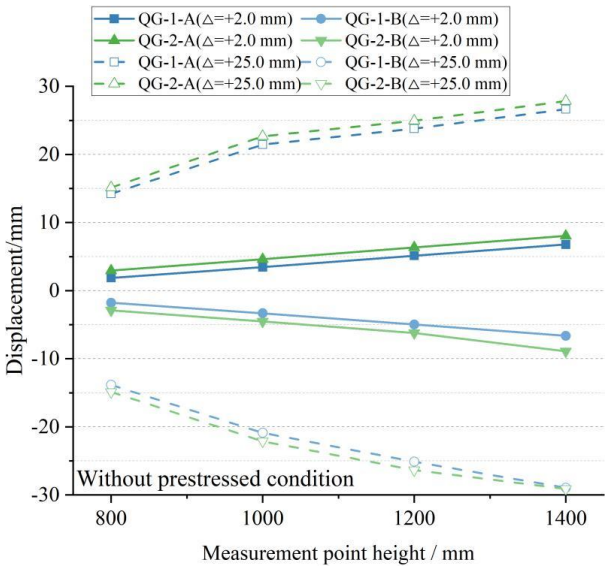

Figure 12: Deformation diagram of wall height without prestressed condition

Without prestressing, the deformation of structural members is generally higher than under prestressed conditions. The results indicate that the free deformation capacity of the wall is stronger when there is no prestress constraint, and the performance advantage of QG-2 specimens is more significant. The synergistic effect of reinforcement is further highlighted. The constraint effect of columns under non prestressed conditions is more prominent, and QG-2 shows a larger deformation increment, indicating that steel reinforcement in a free deformation environment can more efficiently dissipate seismic energy.

3.3.2 Characteristics of Changes in Inter-Wall Spacing

Changes in the distance between walls may consist of the following components: (1) variations in the distance between measurement points caused by the self-deformation of each wall during the loading process; (2) changes in the distance between measurement points due to cracking in the masonry wall near the measurement points; (3) variations in the distance between measurement points resulting from material failure. Furthermore, since the displacement angles at peak load capacity and ultimate load capacity differ for each specimen, this section provides only a qualitative analysis of the changes in distance between walls. Tables 4 and 5 show the distance changes at the measurement points arranged during the peak load capacity stage (Max) and the ultimate load capacity stage (Ultimate) for each specimen, respectively. Here, measurement points A-B are in the compression zone, and B-C are in the tension zone.

Table 4: The change of measurement point distance at max stage

	Location	800mm	1000mm	1200mm	1400mm
QG-1	A-B	-0.12	-0.35	-0.58	-0.82
	B-C	0.08	0.21	0.33	0.45
QG-2	A-B	-0.18	-0.42	-0.67	-0.93
	B-C	0.11	0.26	0.41	0.57
Q-1	A-B	-0.05	-0.14	-0.23	-0.31
	B-C	0.03	0.07	0.12	0.16
Q-2	A-B	-0.09	-0.22	-0.36	-0.5
	B-C	0.06	0.15	0.24	0.33

Table 5: The change of measurement point distance at ultimate stage

	Location	800mm	1000mm	1200mm	1400mm
QG-1	A-B	-1.25	-2.87	-4.52	-6.18
	B-C	0.94	2.13	3.35	4.59
QG-2	A-B	-1.48	-3.26	-5.04	-6.83
	B-C	1.12	2.45	3.78	5.12
Q-1	A-B	-0.62	-1.35	-2.08	-2.81
	B-C	0.41	0.88	1.35	1.82
Q-2	A-B	-0.88	-1.92	-2.96	-3.01
	B-C	0.59	1.27	1.95	2.63

Analysis of the two tables reveals that specimens with structural columns (QG-1, QG-2) exhibit significantly greater changes in measurement point distances at ultimate limit states compared to specimens without structural columns (Q-1, Q-2). As the measurement height increases, the deformation gradually increases, indicating that the deformation of the upper wall part is more obvious. In the final stage, compared with the heights of 800 mm and 1000 mm, all samples show significantly larger deformation at the heights of 1200 mm and 1400 mm, which confirms that the damage is mainly concentrated in the middle and upper wall areas, consistent with the cracking and crushing phenomena observed in the middle and upper parts of the wall during actual seismic events. Overall, structural columns not only greatly improve the deformation capacity and ductility of the wall, but also effectively suppress the propagation of cracks and delay the failure of the structure.

4 Conclusion

This article aims to address the issues of insufficient accuracy and significant deviation from actual seismic damage patterns in traditional empirical statistical methods for predicting seismic damage in masonry structures. A systematic study was conducted on the fusion of mathematical modeling and computer simulation for earthquake damage prediction. (1) Two finite element modeling methods, integral and separated, were compared and analyzed, and a comprehensive modeling strategy that balances efficiency and accuracy was determined based on the requirements of structural macroscopic response analysis; (2) Based on the ABAQUS platform, a concrete damage plasticity (CDP) model is used to describe the constitutive relationship between masonry and concrete materials. A three line hysteresis restoring force model considering stiffness degradation is introduced to construct a nonlinear analysis model suitable for bottom frame masonry structures; (3) The model was validated through quasi-static experiments, and the simulated hysteresis curve, skeleton curve, and stiffness degradation law were in good agreement with the experimental results, with a relative error of less than 3%, proving the accuracy and reliability of the model; (4) By comparing the local deformation and stress characteristics of walls under different construction measures, the dominant role of structural columns in enhancing wall ductility, energy dissipation capacity, and suppressing crack propagation has been clarified.

Next research steps: (1) Introduce the effect of mainshock aftershock sequence to study the impact of cumulative damage on the risk of masonry structure collapse, which is more closely related to the actual earthquake disaster process; (2) By combining machine learning algorithms and utilizing a large amount of simulated data and earthquake damage information to train a vulnerability model for masonry structures, rapid earthquake damage prediction of regional building clusters can be achieved; (3) Considering practical factors such as material degradation and construction defects, further enhance the applicability of the model in engineering scenarios;

(4) Expand the research method to special structural types such as historical masonry buildings and rural masonry houses, forming a seismic damage prediction and safety assessment system covering multiple structural forms and disaster scenarios.

Funding

This work was supported by 2019YFC15090302.

About the Author

Yinghao Xu was born in Xi’an, Shaanxi, China, in 1995. He earned his bachelor's degree from Beijing Jiaotong University and a master's York in the United States. He is currently studying at the School of Civil Engineering of Xi'an University of Architecture and Technology. His primary research focus is on the seismic performance of masonry structures with bottom frames.

References

[1] Lu, X., Cheng, Q., Xu, Z., & Xiong, C. (2021). Regional seismic-damage prediction of buildings under mainshock—aftershock sequence. Frontiers of Engineering Management, 8(1), 122-134.

[2] Boukri, M., Farsi, M. N., Mebarki, A., Belazougui, M., Amellal, O., Mezazigh, B., ... & Benhamouche, A. (2014). Seismic risk and damage prediction: case of the buildings in Constantine city (Algeria). Bulletin of earthquake engineering, 12(6), 2683-2704.

[3] He, Y., Zhai, C., Wen, W., & Zhang, C. (2024). Probabilistic prediction of post-earthquake rubble distribution range for masonry structures. Journal of Building Engineering, 95, 110208.

[4] D’Ayala, D. (2013). Assessing the seismic vulnerability of masonry buildings. In Handbook of seismic risk analysis and management of civil infrastructure systems (pp. 334-365). Woodhead publishing.

[5] Rinaldin, G., & Amadio, C. (2018). Effects of seismic sequences on masonry structures. Engineering Structures, 166, 227-239.

[6] Asteris, P. G., Chronopoulos, M. P., Chrysostomou, C. Z., Varum, H., Plevris, V., Kyriakides, N., & Silva, V. (2014). Seismic vulnerability assessment of historical masonry structural systems. Engineering Structures, 62, 118-134.

[7] Stepinac, M., & Gašparović, M. (2020). A review of emerging technologies for an assessment of safety and seismic vulnerability and damage detection of existing masonry structures. Applied sciences, 10(15), 5060.

[8] Puncello, I., & Caprili, S. (2023). Seismic assessment of historical masonry buildings at different scale levels: a review. Applied Sciences, 13(3), 1941.

[9] Li, S. Q., & Liu, H. B. (2022). Vulnerability prediction model of typical structures considering empirical seismic damage observation data. Bulletin of Earthquake

Engineering, 20(10), 5161-5203.

[10] Morfidis, K., & Kostinakis, K. (2018). Approaches to the rapid seismic damage prediction of r/c buildings using artificial neural networks. Engineering Structures, 165, 120-141.

[11] Siqi, L., Tianlai, Y., & Junfeng, J. (2019). Investigation and analysis of empirical field seismic damage to bottom frame seismic wall masonry structure. International Journal of Engineering, 32(8), 1082-1089.

[12] Erberik, M. A., Citiloglu, C., & Erkoseoglu, G. (2019). Seismic performance assessment of confined masonry construction at component and structure levels. Bulletin of Earthquake Engineering, 17(2), 867-889.

[13] Zhang, S., Liu, Y., & Li, S. (2022). A brief method for rapid seismic damage prediction of buildings based on structural strength. Buildings, 12(6), 783.

[14] Paultre, P., Weber, B., Mousseau, S., & Proulx, J. (2016). Detection and prediction of seismic damage to a high-strength concrete moment resisting frame structure. Engineering Structures, 114, 209-225.

[15] Zhang, J., Bai, Z., Ma, J., Qu, S., Tian, J., Wang, S., & Zhang, R. (2025). Predictive analysis of seismic damage to buildings near-surface faults under the influence of multiple factors. PLoS One, 20(5), e0320930.

[16] Chang, C. M., & Chou, J. Y. (2018). Damage detection of seismically excited buildings based on prediction errors. Journal of Aerospace Engineering, 31(4), 04018032.

[17] Morici, M., Canuti, C., Dall'Asta, A., & Leoni, G. (2020). Empirical predictive model for seismic damage of historical churches. Bulletin of Earthquake Engineering, 18(13), 6015-6037.

[18] Del Gaudio, C., De Risi, M. T., & Verderame, G. M. (2022). Seismic loss prediction for infilled RC buildings via simplified analytical method. Journal of Earthquake Engineering, 26(11), 5477-5510.

[19] Chourasia, A., Bhattacharyya, S. K., Bhandari, N. M., & Bhargava, P. (2016). Seismic performance of different masonry buildings: full-scale experimental study. Journal of Performance of Constructed Facilities, 30(5), 04016006.

[20] Penna, A., Morandi, P., Rota, M., Manzini, C. F., Da Porto, F., & Magenes, G. (2014). Performance of masonry buildings during the Emilia 2012 earthquake. Bulletin of Earthquake Engineering, 12(5), 2255-2273.

[21] Bilgin, H., Shkodrani, N., Hysenlliu, M., Ozmen, H. B., Isik, E., & Harirchian, E. (2022). Damage and performance evaluation of masonry buildings constructed in 1970s during the 2019 Albania earthquakes. Engineering Failure Analysis, 131, 105824.

[22] Mouyiannou, A., Penna, A., Rota, M., Graziotti, F., & Magenes, G. (2014). Implications of cumulated seismic damage on the seismic performance of unreinforced masonry buildings. Bulletin of the New Zealand Society for Earthquake Engineering, 47(2), 157-170.

[23] Gharehbaghi, S., Gandomi, M., Plevris, V., & Gandomi, A. H. (2021). Prediction of seismic damage spectra using computational intelligence methods. Computers & Structures, 253, 106584.

[24] Ferreira, T. M., Estêvão, J., Maio, R., & Vicente, R. (2020). The use of Artificial Neural Networks to estimate seismic damage and derive vulnerability functions for traditional masonry. Frontiers of Structural and Civil Engineering, 14(3), 609-622.

[25] Xu, Z., Wu, Y., Qi, M. Z., Zheng, M., Xiong, C., & Lu, X. (2020). Prediction of structural type for city-scale seismic damage simulation based on machine learning. Applied Sciences, 10(5), 1795.

[26] Morfidis, K., Stefanidou, S., & Markogiannaki, O. (2023). A rapid seismic damage assessment (RASDA) tool for RC buildings based on an artificial intelligence algorithm. Applied Sciences, 13(8), 5100.

[27] Li, S. Q., & Liu, H. B. (2022, May). Statistical and vulnerability prediction model considering empirical seismic damage to masonry structures. In Structures (Vol. 39, pp. 147-163). Elsevier.

[28] Lu, X., Tian, Y., Guan, H., & Xiong, C. (2017). Parametric sensitivity study on regional seismic damage prediction of reinforced masonry buildings based on time-history analysis. Bulletin of Earthquake Engineering, 15(11), 4791-4820.

[29] Su, Q., Cai, G., & Larbi, A. S. (2019). Seismic damage assessment indexes for masonry structures. Journal of Structural Engineering, 145(7), 04019066.

[30] Li, S. Q., Chen, Y. S., Liu, H. B., Du, K., & Chi, B. (2022). Assessment of seismic damage inspection and empirical vulnerability probability matrices for masonry structure. Earthquakes and Structures, 22(4), 387.

[31] De Matteis, G., & Zizi, M. (2019). Seismic damage prediction of masonry churches by a PGA-based approach. International Journal of Architectural Heritage.

[32] Bhatta, S., & Dang, J. (2023). Seismic damage prediction of RC buildings using machine learning. Earthquake Engineering & Structural Dynamics, 52(11), 3504-3527.

[33] Ravichandran, N., Bidorn, B., Mercan, O., & Paneerselvam, B. (2025). Data-driven machine-learning-based seismic response prediction and damage classification for an unreinforced masonry building. Applied Sciences, 15(4), 1686.

[34] Hoveidae, N., Fathi, A., & Karimzadeh, S. (2021). Seismic damage assessment of a historic masonry building under simulated scenario earthquakes: A case study for Arge-Tabriz. Soil Dynamics and Earthquake Engineering, 147, 106732.

[35] Binda, L., Gambarotta, L., Lagomarsino, S., & Modena, C. (2018). A multilevel approach to the damage assessment and the seismic improvement of masonry buildings in Italy. In Seismic damage to masonry buildings (pp. 179-194). Routledge.

[36] Sun, B., & Zhang, G. (2018). Study on vulnerability matrices of masonry buildings of mainland China. Earthquake Engineering and Engineering Vibration, 17(2), 251-259.

[37] Caddemi, S., Caliò, I., Cannizzaro, F., & Pantò, B. (2014, September). The seismic assessment of historical masonry structures. In Proceedings of the 12th International Conference on Computational Structures Technology, Naples, Italy (pp. 2-5).

[38] Gu, X. L., Zhou, T., Nagai, K., Zhang, H., & Yu, Q. Q. (2024). Prediction of seismic performance of a masonry-infilled RC frame based on DEM and ANNs. Engineering Structures, 316, 118531.

[39] Brunelli, A., De Silva, F., Piro, A., Parisi, F., Sica, S., Silvestri, F., & Cattari, S. (2021). Numerical simulation of the seismic response and soil–structure interaction for a monitored masonry school building damaged by the 2016 Central Italy earthquake. Bulletin of Earthquake Engineering, 19(2), 1181-1211.

[40] Jędrzejczyk, A., Firek, K., Rusek, J., & Alibrandi, U. (2024). Prediction of damage intensity to masonry residential buildings with convolutional neural network and support vector machine. Scientific Reports, 14(1), 16256.

[41] Aloisio, A., De Santis, Y., Irti, F., Pasca, D. P., Scimia, L., & Fragiacomo, M. (2024). Machine learning predictions of code-based seismic vulnerability for reinforced concrete and masonry buildings: Insights from a 300-building database. Engineering Structures, 301, 117295.